Chapter 2
Molecular Detection and Force Spectroscopy in Solid-State Nanopores with Integrated Optical Tweezers

Adam R. Hall and Cees Dekker

Abstract We describe how individual biopolymer molecules can be captured, detected and manipulated inside a solid-state nanopore using an integrated optical tweezer system. The combination of nanopore and tweezer technologies offers measurement capabilities like size and length discrimination similar to translocation experiments along with arbitrary position control and the ability to perform direct force spectroscopy. We discuss the experimental setup and measurements on two different types of molecules (bare DNA and protein-coated DNA), and we describe a model for the force on a charged molecule in a nanopore.

Keywords Force Spectroscopy • Integrated Optical Tweezers • Size and length discrimination • Protein-Coated DNA Molecules

2.1 Introduction

Solid-state nanopores show great promise as a high-throughput means by which to detect and analyze biopolymers on an individual basis [1, 2]. A commonly used method towards this end involves the use of a thin, insulating membrane with a single fabricated pore in it (typically prepared by either a transmission electron microscope [3] or a focused ion beam [4]) that acts as a barrier between two supplies of ionic solution. The application of a voltage across the membrane sets up an electric field that is strongly focused inside the pore and can be used to transport charged molecules from one side to the other electrophoretically. Upon doing so,

A.R. Hall (✉)
Kavli Institute of Nanoscience, Delft University of Technology, Lorentzweg 1,
Delft, CJ 2628, The Netherlands
and
Joint School of Nanoscience and Nanoengineering, University of North Carolina
at Greensboro, Greensboro, NC 27401, USA
e-mail: adam.hall@uncg.edu

the presence of the molecule can be detected by monitoring its effect on the trans-membrane current, which is measured by a patch-clamp amplifier.

During electrophoretic translocation, molecules typically pass through the nanopore at high speed. A 48 kbp double-strand DNA (dsDNA) molecule, for instance, traverses the pore in only about 1 ms under an applied voltage of 120 mV [5]. While this presents advantages for some applications (high throughput rapid screening to name one), it poses a challenge for others. For example, accurate detection of submolecular structure like local protein position or even nucleotide sequence – an especially promising goal in the field – would require very high bandwidth to achieve. One potential way to address this is to adjust experimental variables like temperature and viscosity in order to slow down the translocation speed. However, this places inherent limitations on solvent conditions and thus on what can be measured. A more elegant solution would be a mechanism by which to "hold on" to a given molecule and control its position relative to the pore. Such a situation would offer the ability to slow, halt, or even reverse translocation arbitrarily.

Here, we describe a technique that yields this level of control: solid-state nanopores with integrated optical tweezers [6]. We detail how the experiments are performed, describe how the resultant measurements are interpreted, and discuss a model developed along the way that gives insight into the dominant forces involved in nanopore translocation.

2.2 Experimental Methods

Solid-state nanopores are fabricated using a method that has been described elsewhere [7]. Briefly, common microfabrication techniques are used to produce a 20-nm thin, 5 μm wide, free-standing window of silicon nitride supported in a silicon chip. This chip is then mounted in a transmission electron microscope (TEM) and the highly-focused electron beam is used to locally ablate the surface, effectively "drilling" a single hole through the membrane (Fig. 2.1a, inset). The properties of the resultant nanopore (diameter, shape) can be controlled to some degree by adjusting the beam intensity, beam size, and the exposure time [8]. After pore formation, the entire chip is stored in a solution of 50% ethanol in water. The mixture was chosen in order to keep the membrane clean and hydrated, but to allow fluid to wet the interior of the small pore more easily by reducing the surface tension.

Prior to use the chip is cleaned with water, acetone and ethanol, then dried under nitrogen flow and exposed to an oxygen plasma for 30 s in order to create a hydrophilic surface. Directly following this treatment, the chip is introduced with measurement solution (KCl solution with 10 mM tris-HCl at pH 8.0). The sample cell (Fig. 2.1a) is composed of a sandwich-type structure with a poly(methyl methacrylate) (PMMA) flow cell below the chip and a Perspex flow cell above. This allows independent exchange of solvent to both sides of the membrane while still permitting the optical path necessary for optical tweezer integration (Fig. 2.1b). The assembled flow cell is positioned on a three-dimensional piezo stage above a $60\times$ water immersion objective, which acts as the focusing lens of both the optical trapping laser (4 W, $\lambda = 1,064$ nm) and a second position-reading laser (5 mW, $\lambda = 650$ nm) the light of
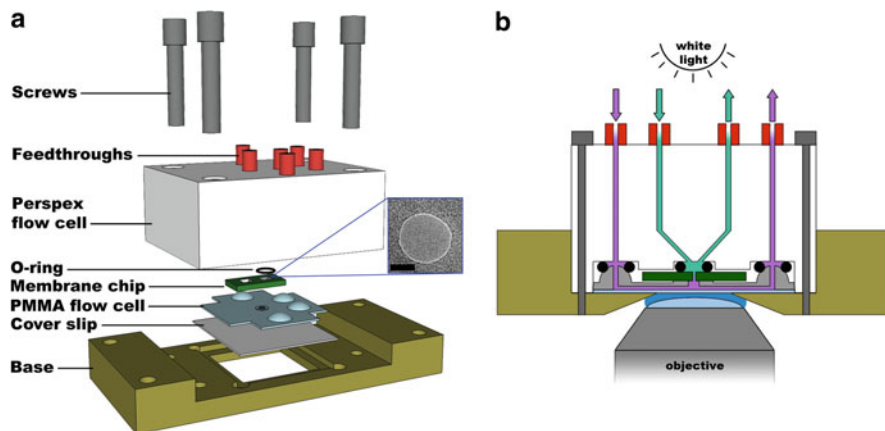
Fig. 2.1 The experimental setup. (**a**) Diagram of the nanopore flow cell, detailing each component. Inset: TEM image of a typical nanopore (scale bar 10 nm). (**b**) Side view of the assembled flow cell, showing the liquid feedthroughs to both the top (*inner*) and bottom (*outer*) of the nanopore chip, and the optical path for transmitted light to the objective

which is reflected onto a position-sensitive detector (PSD). The objective is used additionally as a means for optical feedback using a CCD camera. Electrical contact is made to measurement solutions with agarose salt bridges and Pt connecting wires using small, enclosed reservoirs of 1 M KCl containing 100 mM ferro/ferri cyanide as a redox agent. Voltage application and ionic current measurements are performed using a patch-clamp amplifier (Axopatch 200B). This experimental setup is described in greater detail elsewhere [9].

A given nanopore is tested for linear I–V characteristics (Fig. 2.2a) and low electrical noise (<20 pA RMS) before further use. In the event of unacceptable properties, the pore can be cleaned briefly (~5 min) with 1 M NaOH and/or rinsed, plasma treated and remounted for additional testing. Poor qualities are often the result of bubbles [10] and can also be remedied by exchanging the solution with water and then ethanol before exchanging back to measurement buffer. If all treatments fail, the pore is abandoned and a new chip is used. Nanopores can sometimes be unsuitable for measurement even immediately after fabrication due to unknown reasons. Using the ethanol/water storage conditions, we find that 80% of pores are fit for measurement.

Following identification of a useful nanopore, its precise location on the membrane is determined. This is done by rastering the high-power trapping laser across the membrane surface and monitoring the trans-pore current at each step. As the laser focus comes near the nanopore, it locally heats the solution, increasing its mobility and thus the measured ionic current. The resulting 2D array displays a (nominally gaussian) spike [11] at the location of the nanopore. The membrane is then positioned such that the trapping laser is co-local with the nanopore and moved about 10 μm above the focal plane. Following this, microbeads (2 μm polystyrene) with target molecules attached to them [6] are introduced to the bottom chamber at very low concentration (0.001% w/v). Once a single bead is trapped in the optical
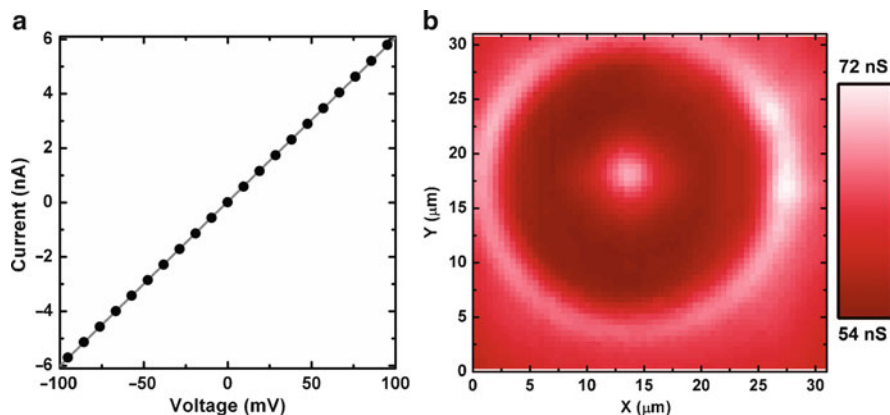
Fig. 2.2 (**a**) Typical I–V measurement on a 8 nm nanopore, demonstrating linear response. (**b**) Measured conductance through the same pore as the trapping laser is rastered across the membrane surface. Local heating increases the ionic mobility when the laser beam is at the pore opening, making its location detectable as the bright peak near $(x, y) = (13, 18 \, \mu m)$

tweezer focus, clean measurement solution is flowed into the chamber to prevent additional beads from entering the trap during subsequent measurement. Since the target molecule is mechanically attached to the bead, the membrane-bead separation must be minimized in order to ensure that the molecule is affected by the applied electric field. Therefore, after rinsing, the membrane is lowered to within a short distance (generally 1–3 µm) of the trapped bead; best results are found with a separation roughly equal to the molecular radius of gyration.

Once positioned correctly, the application of a voltage with appropriate polarity across the membrane will attract molecules toward the nanopore. The size of the necessary voltage varies somewhat, but generally falls between 50 and 150 mV. Too low voltage does not create a strong enough field to pull a molecule into the pore in a practical amount of time, while too high voltage creates the risk of capturing multiple molecules or pulling the bead out of the optical tweezer. Each system and molecule will require finesse to identify the optimal conditions. The capture of a molecule in the nanopore is manifested as a sudden change in the measured transmembrane ionic current together with a (roughly) simultaneous change in the PSD signal, indicating bead motion away from its initial position (Fig. 2.3). When this occurs, the applied voltage is immediately reduced to 10–20 mV; enough to keep the captured molecule from diffusing out of the pore, but too weak to introduce others. At this point, the bead position can be changed relative to the nanopore (by moving the membrane in *z*) without losing the molecule.

Force spectroscopy is performed by increasing the applied voltage in a step-wise fashion while continuously monitoring the bead position via the PSD. Each increase in voltage creates an increased electrophoretic force on the molecule, and thus pulls the microbead farther from its initial position and closer to the membrane. A measurement of the position can be done using a detector scheme in which the PSD signal scales directly with the bead position [12], but the results we describe here utilize a calibration curve taken directly prior to incremental voltage stepping [9, 13].
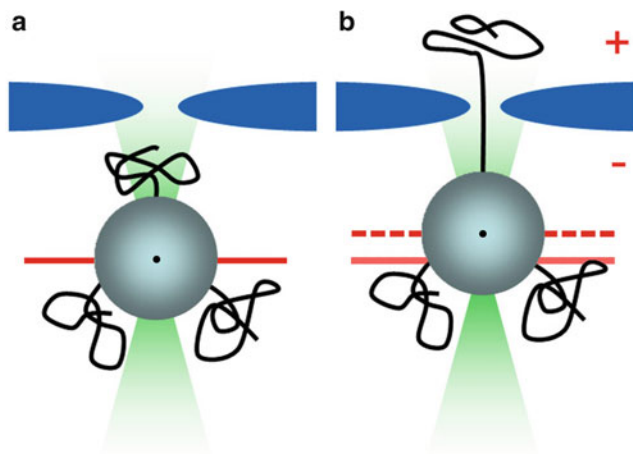
Fig. 2.3 Capturing scheme. (**a**) A microbead (center indicated by *dot*) with target molecules attached is delivered near the nanopore opening with an optical tweezer. (**b**) Upon application of an appropriate voltage, a molecule is pulled in to the pore and held there statically by the optically trapped bead. This action both blocks the nanopore current and displaces the bead from its initial position relative to the membrane (*horizontal lines*)

2.3 DNA Detection

dsDNA (λ-phage, 48.5 kb) is end-labeled through hybridization to a biotin-linked primer with the complimentary 12-base overhang. The resulting material is then attached to streptavidin-coated microbeads with a 1-h incubation at 37°C under buffer conditions of 1 M KCl and 10 mM Tris-HCl (pH 8.0). The concentration of DNA is controlled relative to the beads in order to attach only 1–10 molecules per bead on average. This acts to further reduce the chance of having multiple molecules enter the pore simultaneously.

Captures are performed by applying a voltage across the nanopore membrane while monitoring nanopore current (conductance) and bead position (PSD signal). In order to confirm that target molecules are indeed the cause of such signal changes, a range of applied voltages can be used, as shown in Fig. 2.4a. In this case, the solvent contains 1 M KCl. As increasing positive voltage is applied, dsDNA capture events are eventually observed in both the conductance and the PSD signal (*I, II*). However, by reversing the polarity (*III*), an opposing force is applied which ejects the molecules from the nanopore. Thus, when a positive voltage is applied (*IV*), the original open-pore conductance is again measured until another molecule is eventually captured (*V*) when one returns to negative voltages again.

A closer look at a typical dsDNA capture event is shown in Fig. 2.4b. Two aspects of this measurement bare further mentioning here. First, the amount of conductance change measured (referred to as conductance blockade in high ionic strength conditions [14]) is found to be very consistent at ~1 nS. This is in
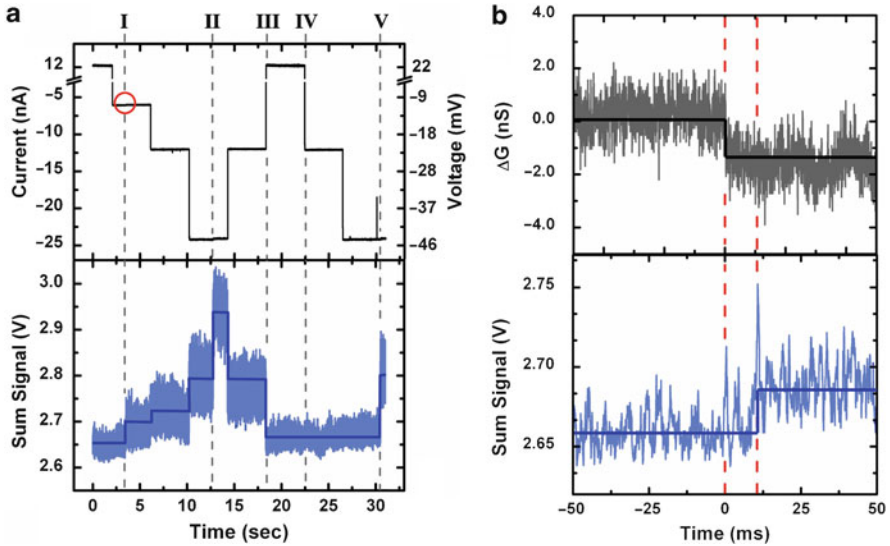
Fig. 2.4 Typical dsDNA captures. (**a**) Simultaneous measurement of nanopore current (*top*) and PSD voltage on the position-sensitive detector (which measures the bead position, *bottom*) under varying applied voltage to the *trans* chamber. See text for descriptions. (**b**) Close-up of the dsDNA capture event circled in (**a**). The *dashed lines* mark the difference in time between the conductance drop (*top*) and the change in bead position (*bottom*)

agreement with the (unfolded) event depth measured in translocation experiments for the same molecule [15] (Fig. 2.5a) and is thus similarly indicative of the size sensitivity of nanopore measurements. Second, although the molecule is statically captured inside the nanopore so the measured conductance does not return to a baseline value as in translocation, temporal information can also be garnered from these optical tweezer measurements. When a molecule is captured in the nanopore, its presence immediately affects the trans-membrane conductance, but there is a delay in the bead position change, because the entire molecule must be threaded through the pore before it is pulled taut and the force is transmitted to the trapped bead. This delay time (Fig. 2.4b, red lines) is a measure of the molecular contour length in the same way that the dwell time is in free translocation [5]. In fact, measurements of the delay consistently match the dwell times for the same length of molecule quantitatively (Fig. 2.5b).

Once a single dsDNA is statically held inside the nanopore, the piezo stage can be used to change the bead-membrane separation and control the position of the molecule relative to the nanopore. An example of this is shown in Fig. 2.6, where the bead is slowly moved away from the membrane surface to a distance greater than the contour length of the molecule (16.5 μm). Here, the measured pore conductance changes suddenly back to the original open-pore level, indicating that the opening is no longer occluded and that the dsDNA has been removed. This occurs at a total distance of 15 μm from the membrane surface, in reasonable agreement with the contour length. The slight difference is due to settling in the system over the long measurement time
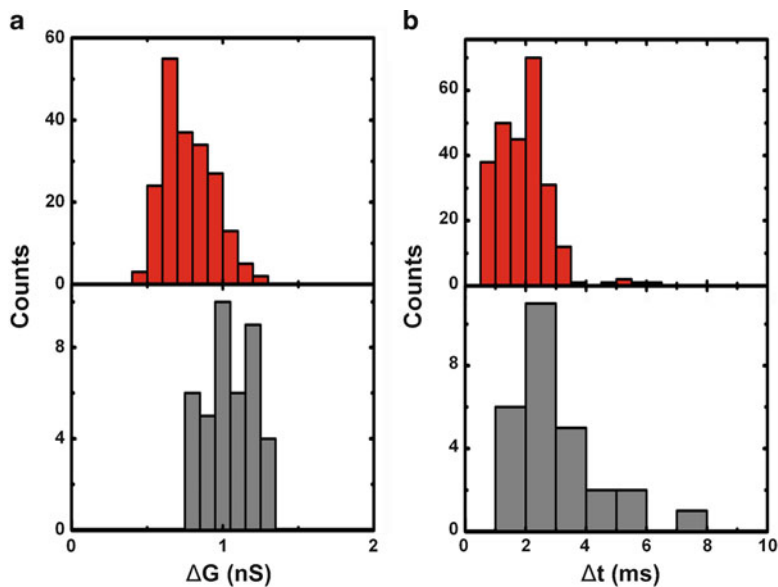
Fig. 2.5 Comparison of translocation to static capturing of dsDNA. (**a**) Conductance change and (**b**) dwell time measurements compared between free translocation (*above*) and static capturing (*below*) [6]
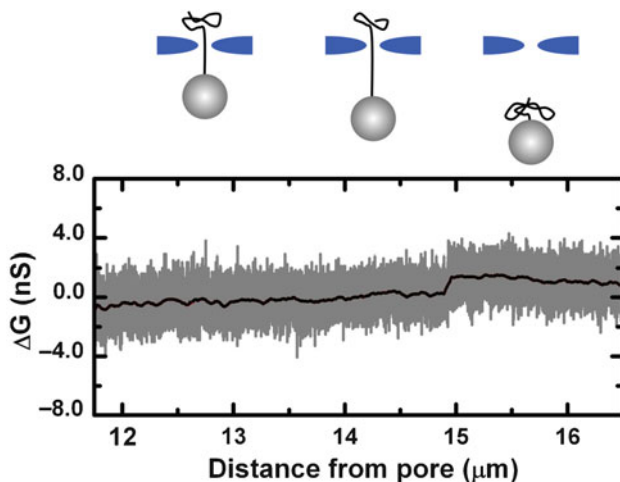

Fig. 2.6 Retraction of captured dsDNA. Measured nanopore conductance as a bead with a captured molecule attached is moved away from the pore using the optical tweezer. At 15 μm, the conductance increases suddenly by ~1 nS, corresponding to the removal of an individual dsDNA from the pore

(largely a result of laser heating of the membrane and optics). The presented retraction is performed at a speed of 20 nm/s; more than five orders of magnitude slower than a common free translocation event (~8 nm/μs).

2.4 Force Spectroscopy

The optically trapped bead can be used as more than merely a handle, however. The net forces acting on the captured molecule are transferred to the bead itself, displacing it from its initial position in the potential well of the optical tweezer. Therefore, changes in force result in relative bead displacements that are measurable through the PSD signal, allowing the system to perform one-dimensional force curves on a single-molecule basis. A typical force curve for dsDNA is shown in Fig. 2.7a (taken in 1 M KCl and at a starting bead-membrane distance of 4 μm), demonstrating the linear relation between applied voltage and measured force.
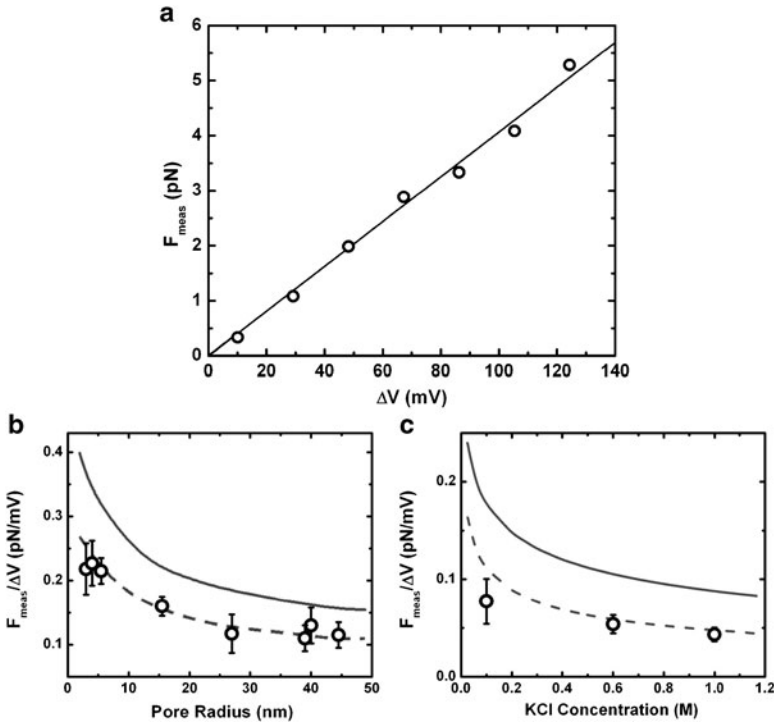

Fig. 2.7 Nanopore force measurements on dsDNA. (**a**) A typical dsDNA force curve (nanopore radius 12 nm, 1 M salt conditions) showing the linear dependence of measured force on applied voltage (*gray line* is a linear fit to the data). The observed relationship between the slope of the force curve and both nanopore radius (**b**) and salt concentration (**c**). The *solid gray line* in each represents the theoretical relation (2) and the *dashed line* represents the same relation calculated with a reduction of dsDNA charge of 50%

Phenomenologically, one can interpret this force as the electrophoretic pulling force $F = Q_{eff}\Delta V$ on the molecule, where Q_{eff} is the effective molecular line charge density and ΔV is the applied voltage [6]. Comparison of the slope of the 1D force curve to the known line charge density of dsDNA (2 e$^-$/bp) would in this view yield a measure of the charge reduction caused by screening in the ionic solution.

Further measurements, however, prove this model to be too simple. The dsDNA force curves, while always linear, are found to vary in slope when performed under different experimental conditions. Particularly, the slope is found to depend on nanopore diameter [16]; smaller pores are found to yield higher levels of force per unit voltage when all other conditions are kept constant (Fig. 2.7b). Concurrently, the ionic strength of the measurement solution is also found to affect the slope [13], with lower molarity salt resulting in greater measured force per unit voltage (Fig. 2.7c). As pure counterion screening should not be changed by shifting in these conditions, the purely electrophoretic model is shown to be incomplete; there must be forces that are unaccounted for in the current description. A revised model [16–19] that captures the results well reveals at least one of those additional forces: electroosmotic drag.

2.5 Modeling: Electrophoresis and Electroosmotic Shear

Charged ions in an electric field experience an electrostatic force. When these ions are in solution, their motion due to this force tends to drag along surrounding liquid molecules. Near a charged surface, the density of counterions is much higher than that of coions, creating a unidirectional net fluid flow in a process called electroosmosis. This effect is especially pertinent to nanopore measurements: because of the small scale, the entire volume contained inside the pore is effectively near a charged surface (the walls of the pore). The introduction of a charged molecule like dsDNA into that confined space will further modify the fluid flow profile. Fluid motion creates a drag force on the captured molecule, affecting the net force acting on it, and it must therefore be accounted for in a model describing the system. The forces used in the present model are detailed in Fig. 2.8a. The net force created by the applied voltage is in fact the electrophoretic force reduced by the electroosmotic drag on the molecule, and it is this combination that is opposed by the restoring force of the optical tweezer.

Ghosal [17] and independently van Dorp et al. [16] showed that the Poisson-Boltzmann relation can be combined with the Stokes equation such that it describes the force on a captured molecule in a nanopore:

$$F_{meas} = \frac{2\pi\varepsilon(\Phi(a) - \Phi(R))}{\ln(R/a)}\Delta V, \tag{2.1}$$
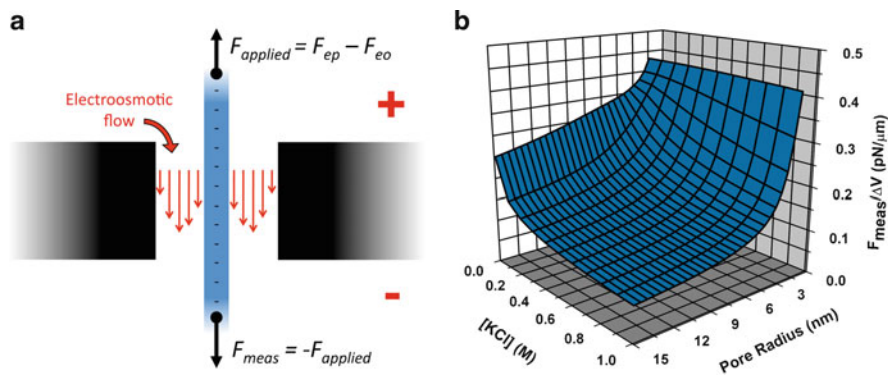
Fig. 2.8 Net electrical forces on a captured dsDNA. (**a**) Diagram of forces on dsDNA (*center*) in a nanopore (*black*), showing that measured force F_{meas} is balanced by a combination of the electrophoretic force (F_{ep}) and the drag force caused by electroosmotic flow (F_{eo}). Flow direction and qualitative magnitude are indicated by the vertical arrows. (**b**) Calculated force curve slope for dsDNA under various ionic concentrations and nanopore radii [2]

where ε is the dielectric constant of water, a and R are radii of the molecule and the nanopore, respectively, and $\Phi(a)$ and $\Phi(R)$ are the surface potentials of the molecule and the nanopore, respectively [17]. A $ln^{-1}(R/a)$ size dependence is therefore predicted, explaining why the measured force is affected by nanopore dimension as observed. Furthermore, the surface potentials are dependent on the distribution of ions surrounding those surfaces; a higher concentration of counterions causes greater screening of surface charge, thereby reducing the surface potential. This is correlated to the overall ion concentration, indicating the source of the observed force dependence on the measurement solution salt concentration.

Comparison of this description to experimental results is achieved by creating a computer model wherein the nanopore is represented by an annulus and the captured molecule by a cylinder, each of uniform charge density. For a designated salt concentration, this allows the ion distribution between the two entities to be calculated numerically. The distribution can then be used to solve the Stokes equation and describe the fluid flow profile, which can subsequently be used to yield the viscous drag acting on the molecule at a given voltage [16]. This can be combined with pure electrophoresis ($F_{EP}=Q\Delta V$) to result in a total prediction of the measured force per unit voltage on a captured molecule for any combination of pore diameter and salt concentration (Fig. 2.8b).

The trends of the size and salt dependences are captured well by the model (Fig. 2.7b, c), but the values do not agree quantitatively; the measured force is apparently overestimated by ~50%. This quantitative difference, while troublesome, has a physical explanation that becomes clearer by comparing these dsDNA measurements to ones on a second type of molecule with different physical properties.

2.6   Measurements on Protein-Coated DNA Molecules

Experiments are also performed by forming a second type of bead-conjugated target molecules: RecA-coated dsDNA [13]. RecA is a protein with an important role in homologous recombination and dsDNA break repair [20]. For the present experiments it was chosen for two main reasons. First, it is able to bind cooperatively along an entire molecule of dsDNA [21], resulting in an uninterrupted coating of protein that can be formed under non-dissociable conditions (upon using ATP-γS). Second, the attachment of this protein coating changes the physical properties of the molecule, the most relevant changes being an increase in diameter (from 2.2 nm for bare dsDNA to ~7 nm for RecA coated dsDNA [22]) and the overall charge (RecA monomers carry a net negative charge).

When nanopore capture experiments are performed on this nucleoprotein filament, the measured change in conductance upon insertion of a molecule is found to differ significantly from that of bare dsDNA under the same experimental conditions. Examples of typical conductance blockades for both kinds of molecule taken in 1 M KCl are shown in Fig. 2.9a. At 1 M KCl, the RecA-dsDNA is found to cause a much larger conductance blockade of about 7 nS, similar to translocation measurements on the same type of molecule [23]. This also agrees qualitatively with the description of how the presence of a molecule affects the measured nanopore conductance [14], wherein the conductance blockade ΔG can be expressed as

$$\Delta G = \frac{1}{L_{pore}} \left(-\pi a^2 (\mu_{cat} + \mu_{an}) n_{tot} e + \mu_{counter} q_l^* \right). \tag{2.2}$$

Here, L_{pore} represents the length of the pore, μ_{cat} and μ_{an} are the electrophoretic mobilities of the cation and anion, respectively, n_{tot} is the total number density of ions in solution, e is the elementary charge, $\mu_{counter}$ is the mobility of counterions near the surface of the molecule (which we adopt to equal the bulk mobility), and q_l^* is the net charge per unit length of carriers surrounding the molecule, which to first order equals the effective line charge density Q_{eff} of the molecule [13]. This expression shows that when the ionic concentration is high (n_{tot} is large), the first term, which scales with the square of the diameter a of the molecule, is dominant, and thus the conductance change is essentially a measure of molecular size. Since RecA-coated dsDNA has a larger diameter than bare dsDNA, it makes sense that the conductance change for the former is greater than the latter.

A more complete comparison can be made by examining the conductance change for each molecule under various salt concentrations (Fig. 2.9). In both cases, measurements indicate a transition from conductance blockades at high ionic strength to conductance enhancement at low ionic strength. A fit to the data [13] for bare dsDNA yields an apparent charge of −0.22 nC/m which compares reasonably with translocation measurements [14] on the same molecule which yielded
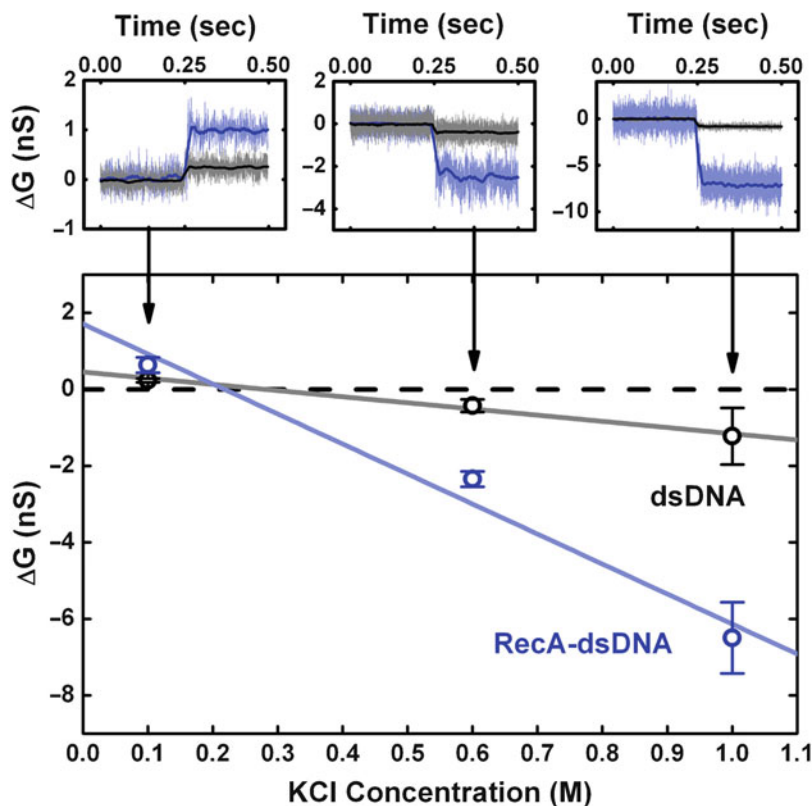
Fig. 2.9 Conductance change during static capture. Measured conductance change upon molecular capture for both bare (*dark points*) and RecA-coated (*light points*) dsDNA under various salt concentrations (*top*). The relation is found to be linear for each (*bottom*) and can be described well by fitting to (2) (*solid lines*) [13]

−0.38 nC/m. As with the force spectroscopy measurements, these analyses show that a reduction from the known line charge density of bare dsDNA (−1.1 nC/m) is necessary to have quantitative agreement between model and experiment. A fit to the conductance changes measured for RecA-coated dsDNA, meanwhile, yields an apparent line charge density of −1.6 ± 0.6 nC/m. When compared with the theoretical nucleoprotein filament charge of −1.8 nC/m (calculated by simple charge summation of the RecA amino acids with the underlying dsDNA [13]), this result indicates that a charge reduction is *not* necessary to achieve quantitative agreement for RecA-dsDNA.

Force spectroscopy is also performed on the protein-coated molecule under multiple ionic strengths (Fig. 2.10a). Several things can be noted from these results. First, the slopes of RecA-dsDNA force curves can be easily distinguished from those of bare dsDNA under all examined conditions. This points toward the ability
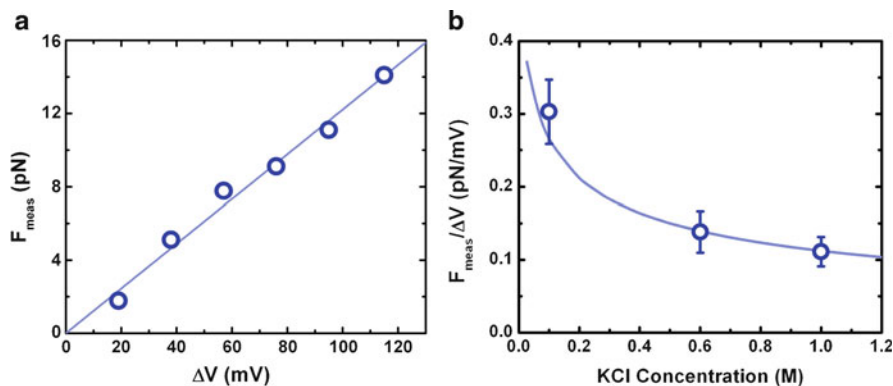
Fig. 2.10 Nanopore force measurements on RecA-dsDNA. (**a**) A typical force curve on RecA-coated dsDNA, taken at 1 M KCl. (**b**) Measured relationship between RecA-dsDNA force curve slope and salt concentration. The *solid line* is the calculated relation with no fitting parameters

of the measurement technique to identify different molecules with a mechanism separate from that of conductance blockade. Second, it is apparent that the force per unit voltage acting on the protein-coated molecule is greater as ionic strength decreases. As with bare dsDNA measurements, this fits qualitatively with the model, which anticipates that lower salt concentration reduces the opposing electroosmotic drag force. Third, and perhaps most importantly, the experimental relation between measured force and salt concentration is described well by the electrophoretic/electroosmotic model without any additional fitting (Fig. 2.10b). As with the conductance change measurements, this suggests that no charge reduction is needed for a RecA-dsDNA molecule.

These results taken in total are suggestive of the source of the deviation between the model and experiments for bare dsDNA. One potential cause is the presence of stationary charges on the surface of the nanopore. However, as the same nanopores were often used to measure both types of molecule presented here, this would produce a systematic variation. Since no adjustment is needed for the fit to the nucleoprotein filament data, this source can be excluded. Instead, a more likely explanation is a reduction in the mobility of counterions close to the molecular surface. Although the RecA-dsDNA molecule has higher total charge than its uncoated counterpart, its larger diameter results in a lower surface charge density (-0.08 C/m^2 compared to -0.14 C/m^2 for bare dsDNA) [13]. Non-linear charge accumulation will therefore cause counterions to interact more strongly with the bare dsDNA surface, reducing their mobility to a larger degree than for the protein-coated molecule. The current understanding of charge screening layers in solution cannot account for such short-range effects. Future experiments could be used to confirm this hypothesis by examining molecules of different surface charge density, such as dsDNA coated with proteins of different charge.

2.7 Conclusions

The combination of optical tweezers with solid-state nanopores represents a versatile system for the study of biomolecules. The use of an optical tweezer to deliver bead-conjugated target molecules to the nanopore allows measurements similar to those measured with pure translocation (size and length discrimination) but additionally presents new capabilities unattainable in traditional systems (arbitrary position control, force spectroscopy). We have demonstrated that measurements on conductance change and dwell time with the combination of technologies allow bare dsDNA to be differentiated from RecA-coated dsDNA, comparable to translocations. However, we have also shown that force curves can be measured on both types molecules, demonstrating the ability to differentiate molecules through a second method in the same system. The dependence of measured force curves on both nanopore dimension and ionic concentration can be described well by a model incorporating both electrophoresis and electroosmosis. This provides a foundation with which to understand the results of forthcoming studies.

Future studies will exploit the position control inherent in the optical tweezer system to allow for this measurement technique to be performed on local structures. Simultaneous detection of both conductance and applied force will allow for a multi-faceted approach to detect small features along an individual biomolecule. This opens the door to, for example, epigenetic footprinting at the molecular scale.

References

1. D. Branton, D. W. Deamer, A. Marziali, H. Bayley, S. A. Benner, T. Butler, M. Di Ventra, S. Garaj, A. Hibbs, X. H. Huang, S. B. Jovanovich, P. S. Krstic, S. Lindsay, X. S. S. Ling, C. H. Mastrangelo, A. Meller, J. S. Oliver, Y. V. Pershin, J. M. Ramsey, R. Riehn, G. V. Soni, V. Tabard-Cossa, M. Wanunu, M. Wiggin and J. A. Schloss, Nature Biotechnology **26** (10), 1146–1153 (2008).
2. C. Dekker, Nature Nanotechnology 2 (4), 209–215 (2007).
3. A. J. Storm, J. H. Chen, X. S. Ling, H. W. Zandbergen and C. Dekker, Nature Materials **2** (8), 537–540 (2003).
4. J. Li, D. Stein, C. McMullan, D. Branton, M. J. Aziz and J. A. Golovchenko, Nature **412** (6843), 166–169 (2001).
5. A. J. Storm, C. Storm, J. H. Chen, H. Zandbergen, J. F. Joanny and C. Dekker, Nano Letters **5** (7), 1193–1197 (2005).
6. U. F. Keyser, B. N. Koeleman, S. Van Dorp, D. Krapf, R. M. M. Smeets, S. G. Lemay, N. H. Dekker and C. Dekker, Nature Physics **2** (7), 473–477 (2006).
7. D. Krapf, M. Y. Wu, R. M. M. Smeets, H. W. Zandbergen, C. Dekker and S. G. Lemay, Nano Letters **6** (1), 105–109 (2006).

  8. M. van den Hout, A. R. Hall, M. Y. Wu, H. W. Zandbergen, C. Dekker and N. H. Dekker, Nanotechnology **21** (11) 115304 (2010).
  9. U. F. Keyser, J. van der Does, C. Dekker and N. H. Dekker, Review of Scientific Instruments **77** (10) 105105 (2006).
 10. R. M. M. Smeets, U. F. Keyser, M. Y. Wu, N. H. Dekker and C. Dekker, Physical Review Letters **97** (8) 088101 (2006).
 11. U. F. Keyser, D. Krapf, B. N. Koeleman, R. M. M. Smeets, N. H. Dekker and C. Dekker, Nano Letters **5** (11), 2253–2256 (2005).
 12. A. Sischka, C. Kleimann, W. Hachmann, M. M. Schafer, I. Seuffert, K. Tonsing and D. Anselmetti, Review of Scientific Instruments **79** (6) 063702 (2008).
 13. A. R. Hall, S. van Dorp, S. G. Lemay and C. Dekker, Nano Letters 9 (12), 4441–4445 (2009).
 14. R. M. M. Smeets, U. F. Keyser, D. Krapf, M. Y. Wu, N. H. Dekker and C. Dekker, Nano Letters **6** (1), 89–95 (2006).
 15. A. J. Storm, J. H. Chen, H. W. Zandbergen and C. Dekker, Phys Rev E Stat Nonlin Soft Matter Phys **71** (5 Pt 1), 051903 (2005).
 16. S. van Dorp, U. F. Keyser, N. H. Dekker, C. Dekker and S. G. Lemay, Nature Physics **5** (5), 347–351 (2009).
 17. S. Ghosal, Physical Review E **76** (6) 061916 (2007).
 18. U. F. Keyser, S. van Dorp and S. G. Lemay, Chemical Society Reviews **39** (3), 939–947 (2010).
 19. J. L. Viovy, Reviews of Modern Physics **72** (3), 813–872 (2000).
 20. S. C. Kowalczykowski, D. A. Dixon, A. K. Eggleston, S. D. Lauder and W. M. Rehrauer, Microbiological Reviews **58** (3), 401–465 (1994).
 21. R. Galletto, I. Amitani, R. J. Baskin and S. C. Kowalczykowski, Nature **443** (7113), 875–878 (2006).
 22. Z. C. Chen, H. J. Yang and N. P. Pavletich, Nature **453** (7194), 489-U483 (2008).
 23. R. M. M. Smeets, S. W. Kowalczyk, A. R. Hall, N. H. Dekker and C. Dekker, Nano Letters **9** (9), 3089–3095 (2009).